11th Australasian Fluid Mechanics Conference
University of Tasmania, Hobart, Australia
14-18 December 1992

UNSTEADY FORCE AND PRESSURE ON A TURBOMACHINE BLADE

Tsutomu ADACHI[1] and Yoshimori MURAKAMI[2]

[1]Institute of Engineering Mechanics, University of Tsukuba, JAPAN

[2]Dept of Mechanical Engineering, Tsukuba College of Technology, JAPAN

Abstract

In this paper, unsteady force and pressure on air-foil in the turbomachinery are studied. At first, the causes of unsteady force are examined by using a single stage axial-flow fan. It is shown that for a proper axial-distance between moving and stationary blade rows the unsteady phenmena arise only from the effect of viscous effects. Unsteady pressure and forces acting on a blade passing through an oblique sinusoidal wake are calculated. Effects of angle of attack, camber and both longitudinal and transverse gust wake are discussed. Dividing wakes by h-sheets of thin wakes with small width and summing them up, unsteady pressure due to wake are calculated and compared with experimental results.

Notations

C	:	chord
C_L	:	lift coefficient
L	:	axial distance between moving and stationary rows
l	:	chord length
U	:	velocity of steady flow
α	:	angle of attack
γ	:	vorticity
ω	:	nondimensional frequency

Suffixes

f	:	camber
g	:	gust
h	:	small width of wake
t	:	time or unsteady
u	:	perturbation velocity in x-direction
v	:	perturbation velocity in y-direction
x	:	x-direction
y	:	y-direction
Δ	:	difference or unsteady

Introduction

In turbomachinery, there are guide vanes, stationary blade rows and moving blade rows making relative movement in a confined area surrounded by a casing and a hub. Flows in these machinery, therefore, become unsteady and dependent also on places. These fluctuations become the cause of vibrations or breakdown of blades, arise in noise and accompany energy losses. From demands for higher efficiency, to prevent vibration or fatigue failure of blades and to decrease noise, much research has been published on the basic problems on the unsteady performance of cascade flow.

The main causes of these interactions are potential flow effects between the moving and stationary blade rows and the viscous effects of shedding from the blades of the preceding stages.

In this paper, at first the causes of fluctuation in the turbomachinery are classified. Then calculations of unsteady pressure are made and compared with experiments and discussions are also made.

INTERFERACTION BETWEEN MOVING AND STATIONARY BLADE ROWS

The authors (1974) investigated the unsteady forces acting on the stationary blades in anaxial-flow blower with a stationary row behind a moving blade row to make an attempt to clarify the causes of these interactions. We made measurements of the unsteady forces on the stationary blades for various axial-distances between moving and stationary blade rows.

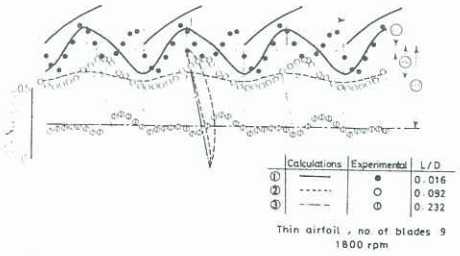

Fig. 1 Fluctuating Phenomena relative to moving blade row.

Figure 1 shows fluctuating phenomena relative to the moving blade row. Three sorts of axial-distances between moving and stationary blade rows are shown(①,②,③). The calculated (lines) and measured values (points) of fluctuatingf orces are taken from the reference lines with lines and points respectively. The direction of force upward corresponds to the fluctuating force from the pressure side to the suction side. For example, at a time t the relative

position of the measured stationary blade is as shown by the broken line and the chords of other blades are shown by the chain lines (for l/D=0.016). In this case, the vertical distances from the line to the reference line shows the magnitude of the fluctuating force and those from the point to the reference line also show that measured. As it is clear from the figure, maximum and minimum point of the fluctuating force arising from potential interaction vary in the direction perpendicular to the cascade of the moving blade. On the other hand, the effect of wake shifts in the direction of the relative stream. If we change the axial-distance, the phase of these two effects also shifts. As it is also clear from these figures, the effect of potential interaction shows a remarkable decrease, on the other hand, that of viscous wake shows a slight decrease with an increase in the axial-distance. For the axial-distance ③ the effect ofp otential interaction disappear and only thato f viscous wake effect can be seen.

UNSTEADY PRESSURE ON A CAMBERED BLADE PASSING THROUGH AN OBLIQUE WAKE

a) Equation of unsteady pressure

The x, y-components of the flow perturbation u_g, v_g can be represented by a sinusoidal wave travelling with the main stream velocity U. Thus,

$$u_g(x,t)=\bar{u}_g(x)\,e^{i\omega t'}=\bar{\bar{u}}_g\,\exp[i\omega(t'-x')],$$
$$v_g(x,t)=\bar{v}_g(x)\,e^{i\omega t'}=\bar{\bar{v}}_g\,\exp[i\omega(t'-x')] \quad \cdots(1)$$

where ω is the nondimensional frequency ($\omega=\nu C/2$). Also the nondimensional time t' and the nondimensional distance x' are

$$t'=2Ut/C, \qquad x'=2x/C \quad \cdots(2)$$

where C denotes the chord length. For the case of a blade that has both camber line

$$y=f[(-2x^2/C)+(C/2)] \quad \cdots(3)$$

and the angle of attack α, under u_g and v_g, as shown in Fig. 2, Nauman and Yeh(1973) have shown the unsteady lift.

On the blade($-1\leq x'\leq 1$), the total vorticity consists of the steady vorticity $\gamma_s(x)$, the bound vorticity $\gamma_b(x,t)$. For inviscid flows, γ_b is related to γ_f by the differential equation

$$\partial(\gamma_b+\gamma_f)/\partial t + U\,\partial\gamma_f/\partial x = 0 \quad \cdots(4)$$

The solution is

$$\bar{\gamma}_f(x)=-i\omega e^{i\omega x'}\int_{-1}^{x'} e^{i\omega x^*}\bar{\gamma}_b(x^*)\,dx^* \quad \cdots(5)$$

Applying Euler's equation of motion in the x-direction to a point on the blade, the unsteady pressure on the blade can be expressed as

$$\Delta\bar{P}(x)=\mp(\rho/2)U\bar{\gamma}_b(x)\mp(\rho/2)\bar{u}_g(x)\gamma_s(x) -(\rho/4)\gamma_s(x)\bar{\gamma}_b(x)-(\rho/4)\gamma_s(x)\bar{\gamma}_f(x) \quad \cdots(6)$$

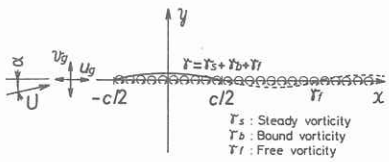

Fig. 2 Cambered blade with angle of attack.

where the upper and lower siogns refer to the suction and pressure sides of the blade, respectively.

Substituting bound vorticity $\gamma_b(x,t)$ and free vorticity $\gamma_f(x,t)$, and using for steady vorticity $\gamma_s(x)$ by the well known result from steady airfoil theory, i.e.,

$$\gamma_s(\theta)=2U\{\alpha\cot(\theta/2)+2f\sin\theta\}, \quad \cdots(7)$$

the final result for ΔP is :

$$\begin{aligned}\Delta\bar{P}(\theta)=&\mp\rho Uf\bar{\bar{u}}_gM_1(\theta,\omega)\mp\rho U\alpha\bar{\bar{u}}_gM_2(\theta,\omega)\\ &\mp\rho U\bar{\bar{v}}_gM_3(\theta,\omega)+\rho Uf\alpha\bar{\bar{u}}_gM_4(\theta,\omega)\\ &+2\rho Uf^2\bar{\bar{u}}_gM_5(\theta,\omega)+\rho U\alpha\bar{\bar{v}}_gM_6(\theta,\omega)\\ &+2\rho Uf\bar{\bar{v}}_gM_7(\theta,\omega)-\rho U\bar{\bar{u}}_gM_8(\theta,\omega).\end{aligned} \quad \cdots(8)$$

In the above equation, $M_1(\theta,\omega)\sim M_8(\theta,\omega)$ are nondimensional unsteady pressure functions, which are defined as

$$\begin{aligned}M_1(\theta,\omega)&=2\sin\theta\,\exp(i\omega\cos\theta)+\phi(\theta,\omega),\\ M_2(\theta,\omega)&=\cot(\theta/2)\exp(i\omega\cos\theta)\\ M_3(\theta,\omega)&=\cot(\theta/2)\,S(\omega)\\ M_4(\theta,\omega)&=\cot(\theta/2)[i\omega\exp(i\omega\cos\theta)\\ &\quad *\int_C^{\theta}\exp(i\omega\cos\theta^*)*\phi(\theta^*,\omega)\sin\theta^*d\theta^*\\ &\quad -\phi(\theta,\omega)]\\ M_5(\theta,\omega)&=\sin\theta\,[i\omega\exp(i\omega\cos\theta)\\ &\quad *\int_C^{\theta}\exp(-i\omega\cos\theta^*)*\phi(\theta^*,\omega)\sin\theta^*d\theta^*\\ &\quad -\phi(\theta,\omega)]\\ M_6(\theta,\omega)&=\cot(\theta/2)\,S(\omega)[i\omega\exp(i\omega\cos\theta)\\ &\quad *\phi(\theta,\omega)-\cot(\theta/2)]\\ M_7(\theta,\omega)&=\sin\theta\,S(\omega)[i\omega\exp(i\omega\cos\theta)\\ &\quad *\phi(\theta,\omega)-\cot(\theta/2)]\\ M_8(\theta,\omega)&=\langle\!\langle 2B_0\{J_0(\omega)\\ &\quad +\sum_{n=2}^{\infty}{}'i^nJ_n(\omega)[\sin n\theta+\sin(n+1)\theta]/\sin\theta\}\\ &\quad -\sum_{n=1}^{\infty}{}'B_n\{\cos m\theta\,[J_0(\omega)+\exp(i\omega\cos\theta)]\\ &\quad +(1/2)\sum_{n=1}^{\infty}i^nJ_n(\omega)\{2\cos(m+n)\theta\\ &\quad +[\sin|(m-n+1)\theta|-\sin|(m-n-1)\theta|]/\sin\theta\}\\ &\quad +2(1-\kappa)\exp(i\omega\cos\theta)\rangle\!\rangle/\kappa\\ \phi(\theta,\omega)&=F(\omega)\cot(\theta/2)\\ &\quad +(4/\omega)\sum_{n=1}^{\infty}i^{n-1}J_n(\omega)\sin n\theta\\ \phi(\theta,\omega)&=\int_C^{\theta}(1+\cos\theta^*)\exp(-i\omega\cos\theta^*)d\theta^*\end{aligned} \quad \cdots(9)$$

and θ is related to x' by $x'=\cos\theta$.

Thus, we see that the unsteady pressure ΔP can be considered as sum of seven terms.

b) Effect of Camber f and angle of attack α on unsteady pressure distribution ΔP

If Re and Im represent the real and imaginary parts of Eq.(8), i.e.,

$$\Delta P(\theta)/(\rho U\bar{\bar{w}}_g)=\mathrm{Re}+i\,\mathrm{Im}$$

$$\Delta Cp=\sqrt{\mathrm{Re}^2+\mathrm{Im}^2}, \quad \phi=\tan^{-1}(\mathrm{Im}/\mathrm{Re}) \quad \cdots(10)$$

Figs. 4～6 show the calculated results for the basic cases of blade under a sinusoidal traveling gust as shown in Fig. 3. For a flat-plate airfoil at zero angle of attack (α=f=0), the unsteady pressure distributions are shown in Fig. 4. The value of ΔCp on both sides of airfoil have the same value at each position along the blade chord, and their chordwise distribution is proportional to $\cot(\theta/2)$. There is no phase lag along the blade chord and the phase difference between the suction and pressure sides is π. Fig. 5 shows the calculated results for the case of the flat-plate airfoil with angle of attack moving through a longitudinal gust. In this case, also, ΔCp on both sides are the same value. Their chordwise distribution is proportional to $\cot(\theta/2)$. The phase difference between both sides is π. Mean while, ΔCp does not decay as ω increases. Fig. 6 shows the results for α=10°, f=0.2 and β=45°, i.e., the cambered blade at angle of attack moving through a longitudinal and transverse gust. In this case, the distributions of values of ΔCp and ϕ vary significantly with β and ω.

As stated above, the unsteady pressure on the cambered blade with angle of attack is very different from that on the flat-plate. It is evident that both the amplitude and the phase vary considerably due to the effects of angle of attack and camber.

c) Extension to arbitrary wake

Consider a blade passing through the wake at an angle β to the x-axis, in Fig. 7. It is assumed that the wake axis passes through the origin of the x, y-coordinate system at the time t=0. Similary to previous studies by Lefcort(1965) and Murakami et al.(1980), it is considered that the wake is devided by h sheets of thin wake with small width Δy_h. Representing the x, y-components of the velocity defect in the wake as a complex Fourier integral, the results are

$$u_g=-(\cot\beta/\pi C)\sum_{h=-\infty}^{\infty} w(y_h)\sum_{k=-\infty}^{\infty}\exp[-i\omega_k(x'-t_h')] * \Delta\omega_k\Delta y_h \quad \cdots(11)$$

$$v_g=-(1/\pi C)\sum_{h=-\infty}^{\infty} w(y_h)\sum_{k=-\infty}^{\infty}\exp[-i\omega_k(x'-t_h')] * \Delta\omega_k\Delta y_h \quad \cdots(12)$$

where, $t_h=(2U/C)(t-y_h/U\sin\beta)$ $\cdots(13)$

Substituting Eqs. (11), (12) for u_g, v_g into Eq. (8), the unsteady pressure ΔP is calculated. In order to reduce the amount of calculation, t_h' in these equations are replaced with x_t', which are fixed points on the x-axis downstream from the leading edge of the blade(see Fig. 9).

Then the unsteady pressure on the blade under the periodic gust are given by

$$\Delta P(\theta)=(\rho U/\pi C)\sum_{x_t=-1}^{1} w(x_t,t') *\cos\beta\ \{\pm fA_1(\theta,x_t')\pm\alpha A_2(\theta,x_t') +f\alpha A_4(\theta,x_t')+2f^2A_5(\theta,x_t')-A_8(\theta,x_t')\} +\sin\beta\ \{\mp fA_3(\theta,x_t')+\alpha A_6(\theta,x_t') +2fA_7(\theta,x_t')\}\ ]\Delta x_t \quad \cdots(14)$$

where A_1～A_8 are response functions and are written in the forms

$$A_1(\theta,x_t')=2\sin\theta F_4(\theta,x_t')+F_5(\theta,x_t'),$$
$$A_2(\theta,x_t')=\cot(\theta/2)F_4(\theta,x_t')$$
$$A_3(\theta,x_t')=\cot(\theta/2)F_3(x_t')$$
$$A_4(\theta,x_t')=\cot(\theta/2)\ [F_5(\theta,x_t')-F_6(\theta,x_t')]$$
$$A_5(\theta,x_t')=\sin\theta\ [F_5(\theta,x_t')-F_6(\theta,x_t')]$$
$$A_6(\theta,x_t')=\cot(\theta/2)\ [F_7(\theta,x_t') -\cot(\theta/2)F_3(x_t')]$$
$$A_7(\theta,x_t')=\sin\theta\ [F_7(\theta,x_t')-\cot(\theta/2)F_3(x_t')]$$
$$A_8(\theta,x_t')=\sum_{k=-\infty}^{\infty} p(\Delta x_t',\omega_k)M_8(\theta,\omega_k) * \exp(i\omega_k x_t')\Delta\omega_k \quad \cdots(15)$$

In the above equations, Equs. F_3～F_7 denote

$$F_3(x_t')=\sum_{k=-\infty}^{\infty} p(\Delta x_t',\omega_k)S(\omega_k)\exp(i\omega_k x_t')\ \Delta\omega_k$$

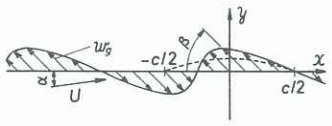

Fig. 3 Cambered blade under a sinusoidal travelling gust w_g.

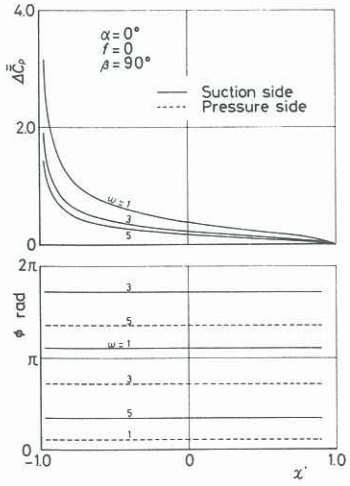

Fig. 4
Unsteady pressure distribution (α=0°, f=0, β=90°).

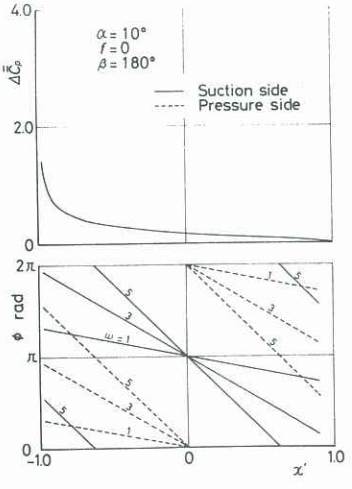

Fig. 5
Unsteady pressure distribution (α=10°, f=0, β=180°).

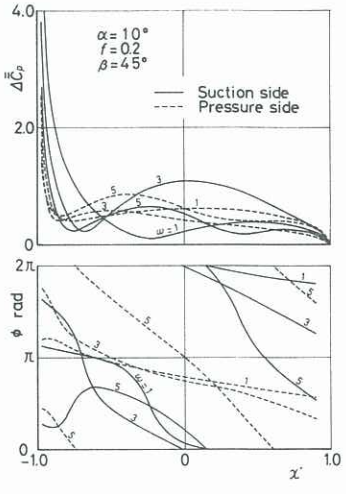

Fig. 6
Unsteady pressure distribution (α=10°, f=0.2, β=45°).

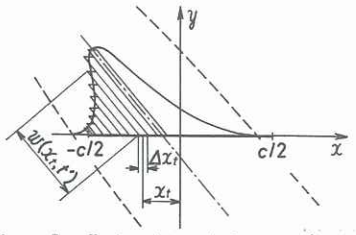

Fig. 7 Velocity defect $w(x_t, t)$ at flat plate.

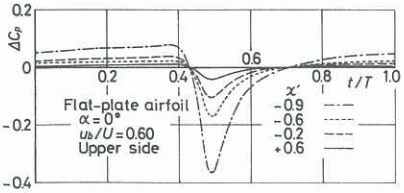

Fig. 8
Unsteady pressure coefficient for a flat plate

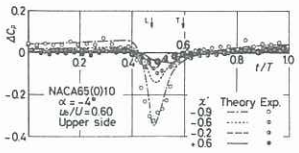

Upper surface

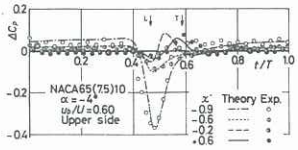

Upper surface

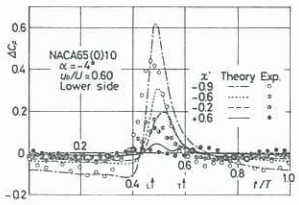

Lower surface

Fig. 9
Comparisons of experimental and measured of unsteady pressure coefficient ΔC_p (NACA65(0)10, $\alpha=-4°$)

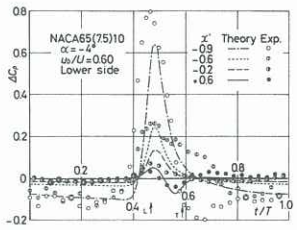

Lower surface

Fig. 10
Comparisons of experimental and measured of unsteady pressure coefficient ΔC_p (NACA65(7.5)10, $\alpha=-4°$)

$$F_4(\theta, x_t') = (2\sqrt{2\pi}/\Delta x_t') * \exp[-2(x_t' + \cos\theta)^2/\Delta x_t'^2]$$

$$F_5(\theta, x_t') = \Sigma p(\Delta x_t', \omega_k)\phi(\theta, \omega_k) * \exp(i\omega_k x_t')\ \Delta\omega_k$$

$$F_6(\theta, x_t') = \Sigma i\omega_k p(\Delta x_t', \omega_k) * \exp[i\omega_k(x_t' - \cos\theta)] * \Sigma\phi(\theta^*, \omega_k)\exp(-i\omega_k\cos\theta^*) * \sin\theta^*\Delta\theta^*\Delta\omega_k$$

$$F_7(\theta, x_t') = \sum_{k=-c}^{c} i\omega_k p(\Delta x_t', \omega_k) S(\omega_k) * \exp[i\omega_k(x_t' + \cos\theta)]\ \phi(\omega_k, \theta)\Delta\omega_k$$

$$\Delta p(\Delta x_t', \omega_k) = \exp(-\Delta x_t'^2\omega_k^2/8) \qquad \cdots(16)$$

Calculated values of $A_1 \sim A_8$ for the fixed point x_t' are used by changing forms of gust $w(x_t, t')$ to get $\triangle p$. In this case, calculations are reduced to that of real values. Calculated values of $A_1 \sim A_8$ are available repeatedly. To show the variation of $\triangle C_p$ with time for the representative four points on the airfoil surface, calculated values of the flat plate with no incidence are shown in Fig. 8. For a flat plate with no incidence placed in the stream, $\triangle p$ [in equation (14)] is expressed by only the term $A_3(\theta, x_t')$. Then the variation of ΔC_p with time show the same form the leading to the trailing edge. Figures 9 and 10 show the comparisons of the calculated results and experimental ones. In these figures, L indicates the time when the center of the wake reaches the leading edge of the blade and T indicates that of the trailing edge of the blade. In the theoretical calculations $\triangle p$ can be expresssed by the sum of A_3 and A_8 in Eq. (14) for flat plate $\alpha=0$. For a airfoil with camber placed with the angle of attack all terms from A_1 to A_8 are related. These results of calculations, which take into account of the blade thickness and the angle of attack, represent the variations of unsteady pressure fairly well.

CONCLUSIONS

These researches are summarised as follows :

1) Interaction effects arise mainly from potential flow effects due to neighboring blades row and from viscous wakes arising from blades upstream. For various axial-distances between the moving and stationary blade rows, the phase difference arising from the above two influences change. The unsteady forces arising from potential flow effects decrease very quickly and those from viscous flow effects decrease slowly with an increase in axial distance.

2) Calculations of unsteady pressure through an oblique sinusoidal wake are calculated. Effects of camber, thickness and angle of attack are shown.

3) Dividing wakes by h sheets of thin wake with small width and adding up, unsteady pressure are calculated and compared with experimental results. Unsteady pressure due to wake of longitudinal and transverse directions, and effects on the cambered, with thickness and also with angle of attack are shown and compared with experiment.

REFERENCES

ADACHI, T, FUKUSADA, Y, TAKAHASHI, N, and NAKAMOTO, Y (1974) Sutdy on the Interference between Moving and Stationary Blade Rows in Axial-Flow Blower. Bulletin of the JSME, 17-109, 904-911.

LEFCORT, M. D, (1965) An Investigation into Unsteady Blade Forces in Turbomachinery. Trans. ASME, J. of Engng. for Power, 87-4, 345-354.

MURAKAMI, Y, HOROSE, T, and ADACHI, T, (1980) Unsteady Force on Blades in a Cascade Due to an Up streamMoving Cylinder(1st Report) Theoretical Calculation, J. of the Japan Society for Aeronautical and Space Sciences, 28-322, 546-554 (in Japanese).

NAUMANN, H, YEH, H, (1973) Lift and Pressure Fluctuations of a Cambered Airfoil under Periodic Gusts and Applications in Turbomachinery. Trans. ASME, J. of Engng. for Power, 95-1, 1-10.